

Emergence of charge density wave and superconducting phase transitions through Lorentz-invariant interactions in the Haldane-Hubbard model

Qiao Yang,^{1,2,*} Yu-Biao Wu^{1,*}, Lin Zhuang,³ Ji-Min Zhao^{1,2,4} and Wu-Ming Liu^{1,2,4,†}

¹Beijing National Laboratory for Condensed Matter Physics, Institute of Physics, Chinese Academy of Sciences, Beijing 100190, China

²School of Physical Sciences, University of Chinese Academy of Sciences, Beijing 100190, China

³State Key Laboratory of Optoelectronic Materials and Technologies, School of Physics, Sun Yat-Sen University, Guangzhou 510275, China

⁴Songshan Lake Materials Laboratory, Dongguan, Guangdong 523808, China



(Received 23 August 2023; revised 12 January 2024; accepted 30 January 2024; published 26 February 2024)

We derive Lorentz-invariant four-fermion interactions, including Nambu-Jona-Lasinio type and superconducting type, which are widely studied in high-energy physics, from the honeycomb lattice Hamiltonian with Hubbard interaction. We investigate the phase transitions induced by these two interactions and consider the effects of the chemical potential and magnetic flux (Haldane mass term) on these phase transitions. We find that the charge density wave and superconductivity generated by the attractive interactions are mainly controlled by the chemical potential, while the magnetic flux delimits the domain of phase transition. Our analysis underscores the influence of the initial topological state on the phase transitions, a facet largely overlooked in prior studies. We present experimental protocols using cold atoms to verify our theoretical results.

DOI: [10.1103/PhysRevB.109.085139](https://doi.org/10.1103/PhysRevB.109.085139)

I. INTRODUCTION

Two-dimensional Dirac materials have emerged as a hot topic in the study of condensed matter physics. The electrons in these materials display a linear dispersion spectrum on the Fermi surface [1]. Despite their fundamentally nonrelativistic nature, their low-energy excitations can be described by the $(2+1)$ -dimensional Dirac equation. This intriguing manifestation blurs the traditional boundaries between relativistic and nonrelativistic realms in the microscopic world, indicating a possible transformation and connection through specific physical systems. However, the challenge lies in effectively bridging these critical aspects of condensed matter models with theoretical models in high-energy physics, thereby forging a pathway for relativistic studies in condensed matter physics. A particularly promising platform to explore this linkage is the Haldane-Hubbard model, setting the stage for the ensuing discussion in this paper.

The Haldane model [2], a classical model of topological insulators, has attracted substantial attention [3–7]. This model describes a two-dimensional honeycomb lattice system with a nonzero Chern number, the characteristics of which have been experimentally verified over the past few years [8]. The Haldane model with interaction has also been extensively studied [9–18]. However, how to connect these essential, experimentally realizable condensed matter models with theoretical models in high-energy physics, and establish a bridge between condensed matter physics and high energy physics, remains an evolving field [19–23]. In high-energy physics, four-fermion

interactions play a crucial role in describing the properties of strongly interacting particles and understanding the low energy limit of the standard model. For example, the Nambu-Jona-Lasinio (NJL) model and Gross-Neveu (GN) model [24–38], are used in the field of particle physics to study meson spectra, color superconductivity, and heavy ion collision physics, etc. And the Thirring model [39–42] is used to study dynamical symmetry breaking, and the phase diagram of real quantum chromodynamics, etc. Most of these models are phenomenological and lack experimental platforms. However, the unique properties of two-dimensional Dirac materials provide us with a unique opportunity to use these materials to simulate these models in high energy physics, particularly those involving interactions that exhibit Lorentz invariance. In this paper, we commence with the Haldane model featuring Hubbard interactions and employ the van der Waerden notation to introduce a mapping from the honeycomb lattice Hamiltonian to a Lagrangian that encompasses two distinct interaction types: NJL type and superconducting type. This notation facilitates the transformation of the nonrelativistic Hubbard interaction into relativistic four-fermion interactions, thus enabling the construction of a fully Lorentz-invariant Lagrangian. We subsequently investigate phase transitions induced by these two interactions by calculating the effective potential. Additionally, we explore the influence of chemical potential and the Haldane mass term (magnetic flux) inherent in the Haldane model on these phase transitions. The Haldane mass term, as widely recognized, has gathered substantial attention in the realm of condensed matter physics and holds significance in high-energy physics. Scholarly studies, such as those found in [12,14,18,43], have delved deeply into the Haldane model in the context of repulsive Hubbard interactions. Simultaneously, the field of high-energy physics, including Refs. [44,45], has explored the connections between

*These authors contributed equally to this work.

†wliu@iphy.ac.cn

the Haldane mass term and Chern-Simons interactions. Our research centers on elucidating the interplay between the topological aspects of the Haldane model and phase transitions induced by weak Hubbard interactions. This area remains relatively unexplored in the existing literature [38,46–49], and our findings offer fresh insights. Notably, we have uncovered that the system, under attractive interactions, can exhibit superconducting and charge density wave (CDW) phases. Furthermore, certain regions of these phase transitions exhibit characteristics that are topologically protected. The pivotal role of the Haldane mass term in influencing the topological attributes of the model within this framework cannot be overstated. Importantly, the Haldane mass term introduced in our study is not an *ad hoc* parameter but naturally emerges from the effective theory of the Haldane model, originating from a physically meaningful quantity associated with magnetic flux $m_o = 3\sqrt{3}t' \sin \phi$. This guarantees the theoretical consistency and practical applicability of our model, offering a fresh perspective on the direct relationship between phase transitions and topology in complex interacting systems. Finally, in the Appendix E, we propose experimental methods for probing these quantum phase transitions using cold atoms.

The rest of the paper is organized as follows. Section II introduces the mapping of the Haldane-Hubbard model to its corresponding Lagrangian, which incorporates both SC-type and NJL-type four-fermion interactions, utilizing van der Waerden notation. Section III is dedicated to the derivation of the system's effective potential. The renormalization analysis of this effective potential is the focus of Sec. IV, where we also present the resultant phase diagram. In Sec. V, we explore the role of the system's initial topological states in modulating interaction-induced phase transitions. Comprehensive derivations of equations cited in the main text can be found in the Appendices.

II. CONSTRUCTING THE LORENTZ-INVARIANT LAGRANGIAN

We study a honeycomb lattice system with nearest-neighbor interactions, contributing to the following spinless Haldane-Hubbard model:

$$\mathcal{H} = \mathcal{H}_0 + \mathcal{H}_T + \mathcal{H}_S + \mathcal{H}_U, \quad (1)$$

with partial Hamiltonian expressed as

$$\mathcal{H}_0 = - \sum_{\langle i,j \rangle} t (a_i^\dagger b_j + \text{H.c.}), \quad (2)$$

$$\mathcal{H}_T = - \sum_{\langle\langle i,j \rangle\rangle} t' (e^{i\phi} a_i^\dagger a_j + e^{-i\phi} b_i^\dagger b_j), \quad (3)$$

$$\mathcal{H}_S = \sum_{i \in A} \mu a_i^\dagger a_i - \sum_{i \in B} \mu b_i^\dagger b_i, \quad (4)$$

$$\mathcal{H}_U = - \sum_{\langle ij \rangle} U a_i^\dagger a_i b_j^\dagger b_j. \quad (5)$$

Here the summation $\sum_{\langle i,j \rangle}$ takes over all nearest-neighbor (NN) sites, and $\sum_{\langle\langle i,j \rangle\rangle}$ takes over all next-nearest-neighbor (NNN) sites. t and t' are real-valued NN and NNN hopping amplitudes, and the latter contain additional phase $\pm\phi$ for different sublattices along the arrows shown in Fig. 1.

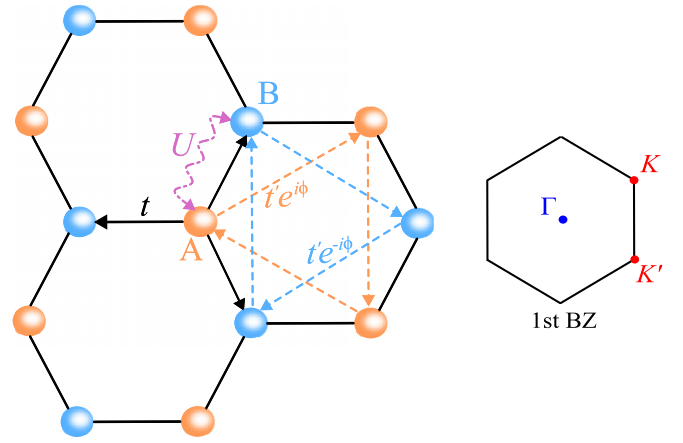


FIG. 1. Haldane model on a honeycomb lattice with nearest-neighbor interactions. The sublattices A and B are represented by orange and blue sites, respectively, each with an energy offset denoted by μ . The real isotropic values are characterized by nearest-neighbor (NN) hopping terms t . The next-nearest-neighbor (NNN) hopping t' is indicated by dashed lines with arrows, incorporating a phase factor $e^{\pm i\phi}$. The interaction U is observed between adjacent particles. The diagram in the right delineates the Brillouin zone, featuring the Dirac points K and K' .

The particle creation and annihilation operators are denoted by $a_i^\dagger (b_i^\dagger)$ and $a_i (b_i)$ for A(B) sublattice. The energy offset μ between sites of A-B sublattices breaks inversion symmetry. U denotes the NN interaction strength between particles in different sublattices. In the following we explain how the Haldane model can be associated with free Dirac fermion Lagrangian, and gives an exact mapping from the Hubbard interaction to those Lorentz invariant four-fermion interactions.

We focus on the NN hopping Hamiltonian \mathcal{H}_0 . From the dispersion relation for the noninteracting theory we obtain six K points, and our choice of two inequivalent ones, which we denote K_\pm , these correspond to the K and K' points in Fig. 1. Expanding around K_\pm , the Hamiltonian \mathcal{H}_0 becomes $H_0 = \int \frac{d^2 p}{(2\pi)^2} (\psi_+^\dagger(p) v_F \sigma \cdot p \psi_+(p) - v_F \psi_-^\dagger(p) (p_x \sigma_x - p_y \sigma_y) \psi_-(p))$, where $\psi_\pm(p) = (a(K_\pm + p), b(K_\pm + p))^T$, $v_F = 3td/2$ (d is the lattice constant). And afterwards, for convenience, we will denote $a(K_\pm + p)$ by a_\pm , and $b(K_\pm + p)$ by b_\pm .

We encapsulate the Hamiltonian of point K and point K' inside a four-component spinor $\Psi^T = (a_+, b_+, b_-, a_-)$. After using the Legendre transformation we can obtain the Lagrangian of the system, $\mathcal{L} = \bar{\Psi} (i\gamma^\nu \partial_\nu) \Psi$, where $\bar{\Psi} = \Psi^\dagger \gamma^0$, $\nu = 0, 1, 2$ and we set $v_F = 1$ for convenience. We use the irreducible four-dimensional spinor representation, the gamma matrices are $\gamma^\mu = \begin{pmatrix} 0 & \bar{\sigma}^\mu \\ \sigma^\mu & 0 \end{pmatrix}$ and $\mu = 0, 1, 2, 3$. There exist one other matrix $\gamma^5 = \begin{pmatrix} 1 & 0 \\ 0 & -1 \end{pmatrix}$, which anticommute with all γ^μ (see Appendix A). We now consider the NNN hopping \mathcal{H}_T and the chemical potential term \mathcal{H}_S . The effective Lagrangian obtained by expanding $\mathcal{H}_T + \mathcal{H}_S$ at the Dirac point K, K' are $\mathcal{L}_m = \psi_\pm^\dagger m_\pm \sigma_z \psi_\pm$. Where $m_\pm = \mu \pm 3\sqrt{3}t' \sin \phi$. For convenience, we set $m_o = 3\sqrt{3}t' \sin \phi$, and it is actually the Haldane mass term [44,50,51]. Now, encapsulate it

inside the four-component spinor, we can get the on-site and Haldane mass terms respectively, $\mu\bar{\Psi}\gamma^3\Psi$, $m_o\bar{\Psi}\gamma^3\gamma^5\Psi$ (see Appendix C). Finally, we can get the free Dirac fermion Lagrangian from the effective theory of Haldane model is $\mathcal{L} = \bar{\Psi}(i\gamma^v\partial_v + \mu\gamma^3 + m_o\gamma^3\gamma^5)\Psi$.

We now consider the Hubbard interaction H_U in continue limit and ignore the interaction between K and K' [52,53]. We take into account the Hubbard interaction for both K and K' point, i.e., $H_U \approx H_{\text{int}} \equiv \int d\mathbf{r} U(a_+^\dagger a_+ b_+^\dagger b_+ + a_-^\dagger a_- b_-^\dagger b_-)$. Following, we will use the van der Waerden notation to map the H_{int} to the Lorentz invariant four-fermion interactions, which contain NJL type and superconducting type. Below we will demonstrate how to create this mapping. We note that $\Psi = \begin{pmatrix} \psi_+ \\ \sigma_1 \psi_- \end{pmatrix}$, and for convenience we define $\chi = \sigma_1 \psi_-$ and $\eta = \psi_+$. Actually, η is the right-chiral Weyl spinor, and the corresponding χ is the left-chiral spinor. Thus, Ψ is indeed a Dirac spinor containing two different chiral Weyl spinors, i.e., $\Psi = \begin{pmatrix} \eta \\ \chi \end{pmatrix}$. We introduce the van der Waerden notation and since we are using the path integral framework, the elements inside Ψ are Grassman numbers rather than operators. According to this notation [54–56], we have $\chi_1 = b_-$, $\chi_2 = a_-$, $\chi^a = \epsilon^{ab}\chi_b$, $\bar{\eta}^1 = a_+$, $\bar{\eta}^2 = b_+$, $\bar{\eta}^a = \epsilon^{ab}\bar{\eta}_b$, where $\epsilon^{12} = \epsilon^{21} = 1$ and $\epsilon_{12} = \epsilon_{21} = -1$. We use the notation $\chi \cdot \chi \equiv \chi^a \chi_a = \chi^\top (-i\sigma_2) \chi$ and $\bar{\chi} \cdot \bar{\chi} \equiv \bar{\chi}_a \bar{\chi}^a = \bar{\chi}^\dagger i\sigma_2 \chi^\dagger$, which are invariant under Lorentz transformation. The Hamiltonian density of the Hubbard interaction can be expressed as $4a_+^\dagger a_+ b_+^\dagger b_+ = (\eta \cdot \eta)(\bar{\eta} \cdot \bar{\eta})$. Similarly, $4a_-^\dagger a_- b_-^\dagger b_- = (\bar{\chi} \cdot \bar{\chi})(\chi \cdot \chi)$. We then introduce a charge conjugate operator $C = -i\gamma^2\gamma^0$, which satisfies $C = -C^{-1} = -C^\dagger$. So, the Hubbard interaction finally can be mapped to the Lorentz invariant four-fermion interactions: $H_{\text{int}} = \frac{U}{4}[(\Psi^\top C \Psi)(\bar{\Psi} C \bar{\Psi}^\top) + (\bar{\Psi} \Psi)^2 - (\bar{\Psi} i\gamma^5 \Psi)^2]$ (see Appendix C).

In the following, we discuss the properties of the model in a more general sense, i.e., using the following Lagrangian:

$$\begin{aligned} \mathcal{L} = & \sum_i \bar{\Psi}_i (i\gamma^v \partial_v + \mu\gamma^3 + m_o\gamma^3\gamma^5) \Psi_i \\ & + \frac{G_1}{N} \left[\left(\sum_i \bar{\Psi}_i \Psi_i \right)^2 - \left(\sum_i \bar{\Psi}_i i\gamma^5 \Psi_i \right)^2 \right] \\ & + \frac{G_2}{N} \left(\sum_i \Psi_i^\top C \Psi_i \right) \sum_j (\bar{\Psi}_j C \bar{\Psi}_j^\top). \end{aligned} \quad (6)$$

Here, we have adopted the large- N assumption that all fermion fields $\Psi_i (i = 1, \dots, N)$ form a fundamental multiplet of the $O(N)$ group. This model is similar to those investigated in Refs. [38,46–49], but we consider the effect of the Haldane mass term, an aspect not addressed in these references. Our assumption $G_1 = G_2 = \frac{U}{4}$ are derived from Hubbard interaction rather than a direct phenomenological parameter, and all the order parameters representing phases that we discuss subsequently originate from genuine condensed matter systems. It is worth mentioning that in this paper, we adopt a distinct gamma matrix representation. However, as we will demonstrate below, the physical results are independent of the representation chosen for the gamma matrices. And in the main text, we will only consider the

parts that are directly related to the Hubbard interaction, i.e., $G_1 = G_2 = G$.

III. EFFECTIVE POTENTIAL

We use the Hubbard-Stratonovich (HS) transformation to decouple these four-fermion interactions and solve for the thermodynamic potential (TDP). We focus on the case with Hubbard interaction, where we set $G_1 = G_2 = G$ and $G = U/4$. Introducing the auxiliary fields Δ , π , σ , we have

$$\begin{aligned} \mathcal{L} = & \bar{\Psi}_i (i\gamma^v \partial_v + \mu\gamma^3 + m_o\gamma^3\gamma^5 - \sigma - i\gamma^5 \pi) \Psi_i \\ & - \frac{N}{4G} (\sigma^2 + \pi^2) - \frac{N}{4G} \Delta^* \Delta - \frac{\Delta^*}{2} \Psi_i^\top C \Psi_i - \frac{\Delta}{2} \bar{\Psi}_i C \bar{\Psi}_i^\top. \end{aligned} \quad (7)$$

Using the Euler-Lagrange equations of motion for these auxiliary fields, which take the form $\sigma(x) = -2\frac{G}{N}(\bar{\Psi}_i \Psi_i)$, $\pi(x) = -2\frac{G}{N}(\bar{\Psi}_i i\gamma^5 \Psi_i)$ and $\Delta(x) = -2\frac{G}{N}(\Psi_i^\top C \Psi_i)$. The ground state expectation values $\langle \Delta(x) \rangle$, $\langle \pi(x) \rangle$, $\langle \sigma(x) \rangle$ of the composite bosonic fields are determined by the saddle point equations,

$$\frac{\delta \mathcal{S}_{\text{eff}}}{\delta \sigma(x)} = 0, \quad \frac{\delta \mathcal{S}_{\text{eff}}}{\delta \Delta(x)} = 0, \quad \frac{\delta \mathcal{S}_{\text{eff}}}{\delta \pi(x)} = 0. \quad (8)$$

Where

$$\exp(i\mathcal{S}_{\text{eff}}(\sigma, \Delta, \Delta^*)) = \int \prod_{l=1}^N [d\bar{\psi}_l][d\psi_l] \exp\left(i \int \mathcal{L} d^3x\right). \quad (9)$$

For simplicity, throughout the paper we suppose that the above-mentioned ground state expectation values do not depend on space-time coordinates, $\langle 0|\sigma(x)|0 \rangle \equiv \sigma$, $\langle 0|\pi(x)|0 \rangle \equiv \pi$, $\langle 0|\Delta(x)|0 \rangle \equiv \Delta$. So, in the leading order of the large- N expansion, after integrating out the fermionic field, we can derive the TDP,

$$\Omega = \frac{\sigma^2 + \pi^2}{4G} + \frac{\Delta^2}{4G} + \frac{i}{2} \sum_i \int \frac{d^3p}{(2\pi)^3} \ln \lambda_i(p), \quad (10)$$

where Δ is a real number, $\lambda_i(p) (i = 1, 2, 3, 4)$ is the four roots of the four-by-four matrix $\mathcal{D}(p) = -\Delta^2 \mathbf{I} + \mathcal{D}_+ \mathcal{D}_-$ (see Appendix B). Without loss of generality, for chiral symmetry breaking, we can always choose a direction such that $\pi = 0, \sigma \neq 0$. In powers of p_0 , we can write $\prod_i \lambda_i(p) = P^+(p_0)P^-(p_0)$. According to the general theorem of algebra, the polynomial $P^\beta(p_0) (\beta = +, -)$ can be presented in the form

$$P^\beta(p_0) = (p_0 - p_{01}^\beta)(p_0 - p_{02}^\beta)(p_0 - p_{03}^\beta)(p_0 - p_{04}^\beta). \quad (11)$$

Then, the TDP is

$$\Omega = \frac{\sigma^2}{4G} + \frac{\Delta^2}{4G} + \frac{i}{2} \sum_\beta \int \frac{d^3p}{(2\pi)^3} \ln P^\beta(p_0). \quad (12)$$

Using the general formula $\int_{-\infty}^{\infty} dp_0 \ln(p_0 - R) = i\pi|R|$. Where R is a real quantity, it is possible to reduce the TDP to the following: $\Omega \equiv \Omega^{un}(\Delta, \sigma) = \frac{\sigma^2}{4G} + \frac{\Delta^2}{4G} - \frac{1}{4} \sum_{\beta, i} \int \frac{d^2\mathbf{p}}{(2\pi)^2} (|p_{0i}^\beta|)$.

IV. RENORMALIZATION AND PHASE DIAGRAM

First, we will obtain a finite (i.e., renormalized) expression for the TDP at $m_o = 0$ and $\mu = 0$. That is, in vacuum,

$$V^{un}(\Delta, \sigma) = \frac{\sigma^2}{4G} + \frac{\Delta^2}{4G} - \int \frac{d^2\mathbf{p}}{(2\pi)^2} (\sqrt{\mathbf{p}^2 + (\Delta + \sigma)^2} + \sqrt{\mathbf{p}^2 + (\Delta - \sigma)^2}). \quad (13)$$

Next, let us regularize the effective potential by cutting momenta; we suppose that $|\mathbf{p}| < \Lambda$. (Note here that we take a spherical coordinate truncation instead of the square truncation in Ref. [46], so there is a difference in the sense of constants). As a result, we have the following regularized expression, which is finite at finite values of Λ :

$$V^{un}(\Delta, \sigma) = (\sigma^2 + \Delta^2) \left(\frac{1}{4G} - \frac{\Lambda}{2\pi} \right) - \frac{\Lambda^3}{3\pi} + \frac{1}{6\pi} (|\Delta + \sigma|^3 + |\Delta - \sigma|^3). \quad (14)$$

We assume that the bare coupling constants G depend on the cutoff parameter of Λ in the way that in the limit $\Lambda \rightarrow \infty$ yields a finite expression in square brackets (14). Obviously, in order to satisfy this requirement, it is sufficient to require that $\frac{1}{4G} \equiv \frac{1}{4G(\Lambda)} = \frac{\Lambda}{2\pi} + \frac{1}{2\pi g}$, where g is finite and Λ -independent model parameter with dimensionality of inverse mass. Ignore there an infinite σ - and Δ -independent constant $-\frac{\Lambda^3}{3\pi}$, one obtains the following renormalization, i.e., finite expression for the effective potential: $V^{\text{ren}}(\Delta, \sigma) = \lim_{\Lambda \rightarrow \infty} \{V^{un}(\Delta, \sigma)|_{G(\Lambda)} + \frac{\Lambda^3}{3\pi}\}$. It should also be mentioned that the V^{ren} is a renormalization group invariant quantity. Finally, we get

$$V^{\text{ren}}(\Delta, \sigma) = \frac{\sigma^2}{2\pi g} + \frac{\Delta^2}{2\pi g} + \frac{1}{6\pi} (|\Delta + \sigma|^3 + |\Delta - \sigma|^3). \quad (15)$$

The coordinates of the global minimum point (Δ_0, σ_0) of the effective potential $V^{\text{ren}}(\Delta, \sigma)$ define the ground-state expectation values of auxiliary fields $\sigma(x)$ and $\Delta(x)$, namely, $\sigma_0 = \langle 0|\sigma(x)|0 \rangle$ and $\Delta_0 = \langle 0|\Delta(x)|0 \rangle$. The quantities σ_0 and Δ_0 are usually called order parameters, or gaps. Moreover, the gap σ_0 is equal to the dynamical mass of one-fermionic excitations of the ground state. That is, its appearance is associated with chiral symmetry breaking. In this work, originating from genuine condensed matter systems, the specific pairing of σ arises from the particle-hole pairing located at two inequivalent Dirac points, leading to the charge density wave (CDW) (see Appendix C). The emergence of Δ_0 is associated with the onset of the superconducting phase transition. It is worth noting that although the regularization scheme we adopt and the representation of the gamma matrix are different from those in Ref. [46], the final resulting effective potential is indeed

precisely the same, so does the phase portrait. This demonstrates that the effective potential is indeed a renormalization group invariant quantity, and it confirms that the physics of the system is independent of the representation chosen for the gamma matrices.

We now study the influence of the Haldane mass term m_o and the chemical potential μ on the phase structure of the model. We have (see Appendix B)

$$\Omega^{\text{ren}}(\Delta, \sigma) = \frac{\sigma^2}{2\pi g} + \frac{\Delta^2}{2\pi g} + \frac{1}{12\pi} (|\Delta + m_o + \sqrt{\mu^2 + \sigma^2}|^3 + |\Delta + m_o - \sqrt{\mu^2 + \sigma^2}|^3 + |\Delta - m_o + \sqrt{\mu^2 + \sigma^2}|^3 + |\Delta - m_o - \sqrt{\mu^2 + \sigma^2}|^3). \quad (16)$$

By solving the extreme points of the given TDP, we can derive the system's phase diagram, which is determined by the interplay of three parameters (g, μ, m_o). We find that in the repulsive region ($g > 0$), no spontaneous symmetry breaking occurs. Conversely, in the attractive region ($g < 0$), the system undergoes spontaneous symmetry breaking, leading to a transition from the CDW to superconductivity. Similar to previous studies that have incorporated chemical potential effects in the context of attractive Hubbard interactions [57–59], the chemical potential in our model also induces superconducting phase transitions. However, the region exhibiting superconductivity in our model is quite peculiar, manifesting only at the phase boundary. Furthermore, the chemical potential μ plays a pivotal role in inducing transitions to both the superconducting phase and the charge density wave (CDW). Meanwhile, the Haldane mass term merely triggers the system's transition process from a symmetric phase to a mixed phase. The corresponding phase diagrams are shown in Fig. 2.

Next, we plotted the phase diagrams of the (g, m_o) and (g, μ) systems, where $(\mu = 0, m_o = 0)$ correspond to Figs. 2(b) and 2(c), and the equations of the corresponding boundary curves of these two plots are $g = -\frac{1}{|\mu|}$ and $g = -\frac{1}{2|m_o|}$, respectively. We find that when $\mu = 0$, under attractive interaction, tuning m_o from negative to positive leads the system to undergo phase transitions from symmetric phase to mixed phase and back to symmetric phase. On the other hand, at $m_o = 0$, adjusting the chemical potential μ induces the system to experience phase transitions from a symmetry phase to a superconducting phase, followed by the emergence of CDW (apart from the line at $\mu = 0$, where the system is in a mixed phase) and then back to symmetry. This suggests that the chemical potential μ strongly induces the emergence of CDW in the system, while the Haldane mass term merely restricts the range of symmetry breaking. In the Appendix D, we also draw the phase diagrams for (g, μ) and (g, m_o) with m_o and μ not equal to 0, respectively. In order to compare with the experiment, we also plotted the order parameters as a function of magnetic flux and chemical potential, see Fig. 3, where (a) and (b) is the thermal diagrams of $\sigma_0(g, \mu) = \sqrt{1/g^2 - \mu^2}$ and $\Delta_0(g, \mu) = \frac{-1/g + \sqrt{1/g^2 - 4\mu^2}}{2}$, respectively ($m_o = 0$ in this

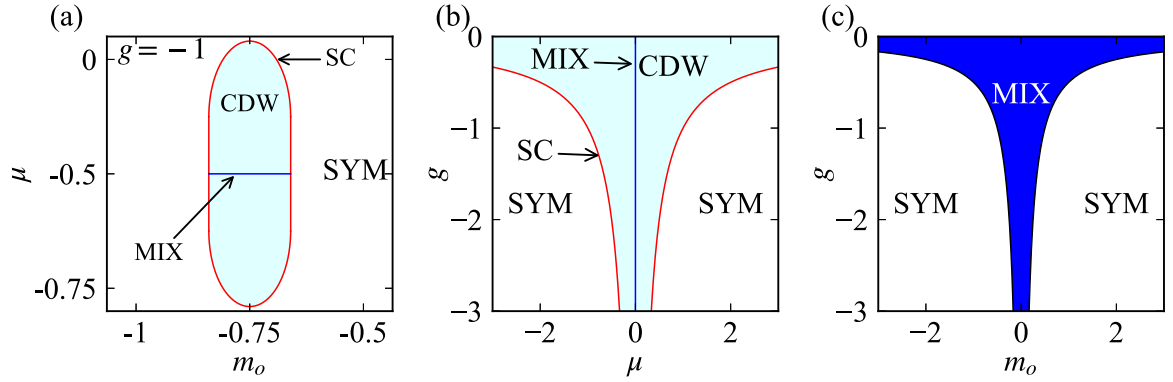


FIG. 2. The phase diagrams of the system under various fixed parameters. (a) The phase diagram in the (μ, m_o) parameter space, where the interaction strength $g = -1$. (b) The phase diagram in the (g, μ) parameter space, where the Haldane mass term $m_o = 0$. (c) The phase diagram in the (g, m_o) parameter space, where the chemical potential $\mu = 0$. In the diagrams, the white area denotes the system in a symmetry (SYM) phase, the sky-blue area represents the system in a CDW phase, the red area indicates the system is in a superconductor (SC) phase, and the blue area signifies the system is in a mixed (MIX) phase of CDW and superconductivity.

case). Figure 3(c) is the thermal diagrams of $\sigma_0(g, \phi) = \Delta_0(g, \phi) = \frac{-1/g + \sqrt{1/g^2 - 4(3\sqrt{3}t \sin \phi)^2}}{2}$ (where we have set $t = 1$ and $\mu = 0$).

V. UNVEILING THE CORRELATION: INITIAL TOPOLOGICAL STATES AND (g_1, g_2) INTERACTION-INDUCED PHASE TRANSITIONS

In this section, we undertake a comprehensive analysis of the system's phase diagram in the (g_1, g_2) parameter space, we analyze the phase structure in the planes defined by the parameters (g_1, g_2) . Furthermore, we will investigate the relationship between the initial topological state of the system and the phase transitions induced by interactions. Remarkably, this specific aspect remains unexplored in the existing literature. We recognize that the topology of the Haldane model is determined by the Chern number: $C = \frac{1}{2}(\text{sgn}(\mu + m_o) - \text{sgn}(\mu - m_o))$, which depends on the relative magnitude of the chemical potential and the Haldane mass term. Specifically, when $\mu > m_o$, $C = 0$ and the system resides in a topologically trivial state; when $\mu < m_o$, $C = 1$ and the system becomes a topological insulator. [Due to the symmetry of the thermodynamic potential (16), i.e., it remains invariant when $\mu \rightarrow -\mu$ and $m_o \rightarrow -m_o$, we limit our discussion to the cases with $m_o > 0$, $\mu > 0$, and $C \geq 0$.] We first discuss two extreme

scenarios: (1) $m_o \neq 0$, $\mu = 0$; (2) $m_o = 0$, $\mu \neq 0$. These cases correspond to two distinct topological states ($C = 1, 0$). Using Eq. (16), we derive the respective thermodynamic potentials (TDP) as follows:

$$\begin{aligned}
 V_{m_o} &\equiv \Omega^{\text{ren}}(\Delta, \sigma, m_o) \\
 &= \frac{\sigma^2}{2\pi g_1} + \frac{\Delta^2}{2\pi g_2} + \frac{1}{12\pi} (|\Delta + m_o + \sigma|^3 \\
 &\quad + |\Delta + m_o - \sigma|^3 + |\Delta - m_o + \sigma|^3 \\
 &\quad + |\Delta - m_o - \sigma|^3), \\
 V_{\mu} &\equiv \Omega^{\text{ren}}(\Delta, \sigma, \mu) \\
 &= \frac{\sigma^2}{2\pi g_1} + \frac{\Delta^2}{2\pi g_2} \\
 &\quad + \frac{1}{6\pi} (|\Delta + \sqrt{\mu^2 + \sigma^2}|^3 + |\Delta - \sqrt{\mu^2 + \sigma^2}|^3). \quad (17)
 \end{aligned}$$

Solving the system of equations, $\begin{cases} \frac{\partial V_i}{\partial \Delta} = 0, \\ \frac{\partial V_i}{\partial \sigma} = 0. \end{cases}$ ($i = m_o, \mu$), we analytically determine the system's order parameters and the conditions for phase boundaries in these two extreme scenarios. The corresponding phase diagrams are depicted below.

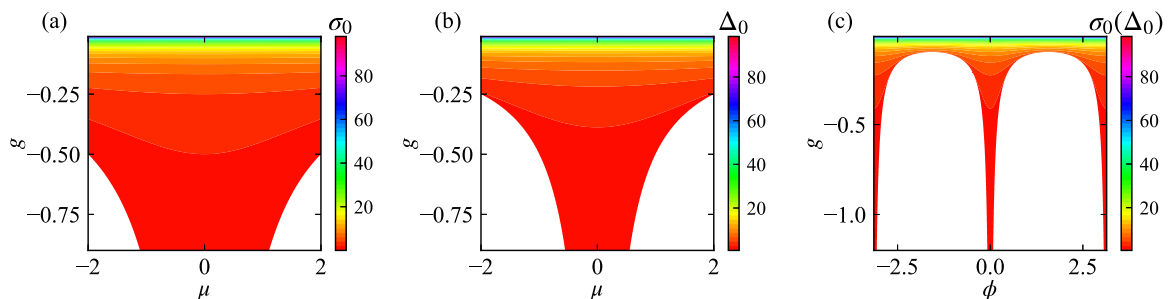


FIG. 3. Thermal diagrams of order parameters vs interaction g and chemical potential μ or magnetic flux ϕ (Haldane mass m_o), respectively. [(a),(b)] Thermal diagrams of the order parameters σ_0 , Δ_0 in the parameter space (g, μ) , respectively. (c) Thermal diagrams of the order parameters σ_0 , Δ_0 in the parameter space (g, ϕ) , where $\sigma_0 = \Delta_0$.

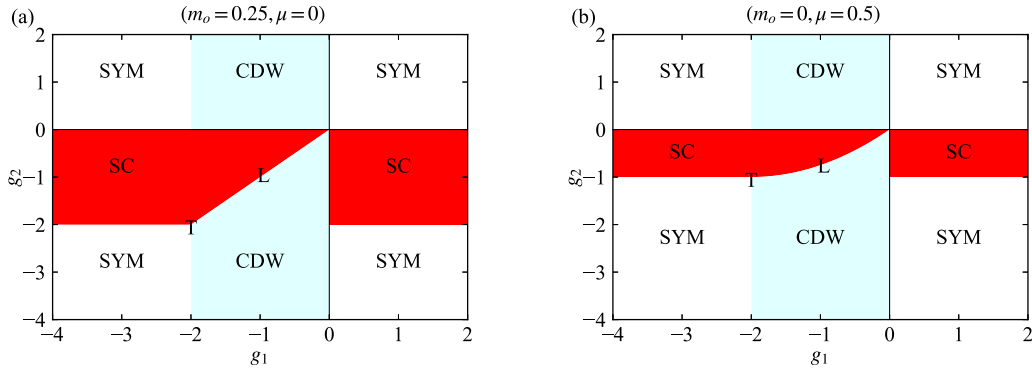


FIG. 4. The (g_1, g_2) -phase portrait of the model. The T point denotes the tricritical point, and the line labeled as L represents the phase boundary in the third quadrant. (a) The (g_1, g_2) -phase portrait at $(m_o = 0.25, \mu = 0)$. (b) The (g_1, g_2) -phase portrait at $(m_o = 0$ and $\mu = 0.5)$.

Figure 4(a) presents the (g_1, g_2) phase diagram in the topological insulator state, where the analytically derived tricritical point T is located at $g_1 = g_2 = -\frac{1}{2|m_o|}$. The superconducting

order parameter $\Delta_0(m_o) = \frac{-\frac{1}{g_2} + \sqrt{\frac{1}{g_2^2} - 4m_o^2}}{2}$ and the CDW order parameter $\sigma_0(m_o) = \frac{-\frac{1}{g_1} + \sqrt{\frac{1}{g_1^2} - 4m_o^2}}{2}$. Figure 4(b) depicts the

(g_1, g_2) phase diagram in the topologically trivial state, with the tricritical point T located at $g_1 = -\frac{1}{|\mu|}, g_2 = -\frac{1}{2|\mu|}$. The

superconducting order parameter $\Delta_0(\mu) = \frac{-\frac{1}{g_2} + \sqrt{\frac{1}{g_2^2} - 4\mu^2}}{2}$ and the CDW order parameter $\sigma_0(\mu) = \sqrt{\frac{1}{g_1^2} - \mu^2}$.

Upon comparing Figs. 4(a) and 4(b), it is evident that the expressions for the triple point T differ in these two extreme scenarios. This observation leads us to pose a question: Is the coordinate of the triple point T related to the topology of the system? Specifically, when the initial system is in a topological state, is the coordinate of T topologically protected? The answer is affirmative; the coordinate of the triple point T is indeed topologically protected. We have demonstrated this by numerically solving the phase diagram of the system when both μ and m_o are simultaneously nonzero, thereby proving that the coordinate of the triple point T is topology-dependent. The numerical phase diagram is presented in Figs. 5 and 6.

When the system initially resides in a topological insulator state, i.e., $\mu < m_o$, the expression for the coordinates of the triple point in the (g_1, g_2) plane remains constant at $(-\frac{1}{2|m_o|}, -\frac{1}{2|m_o|})$, irrespective of the value of the chemical potential μ . Furthermore, the phase boundary L is a straight line.

Conversely, when the system initially resides in a topologically trivial state, i.e., $\mu > m_o$, the expression for the

TABLE I. Coordinates of the triple point T in the (g_1, g_2) plane and geometry of the phase boundary L.

Chern Number	$C = 1$	$C = 0$
Coordinates of T in the (g_1, g_2) plane	$(-\frac{1}{2 m_o }, -\frac{1}{2 m_o })$	$(-\sqrt{\frac{1}{\mu^2 + 2m_o^2}}, -\frac{1}{2 \mu })$
Geometry Of The Phase Boundary L	The Line $g_2 = g_1$	Curve

coordinates of the triple point in the (g_1, g_2) plane becomes $(-\sqrt{\frac{1}{\mu^2 + 2m_o^2}}, -\frac{1}{2|\mu|})$, and the phase boundary L becomes a curve.

Therefore, the topology of the system not only protects the coordinates of the triple point T induced by interaction-induced phase transitions but also preserves the geometric shape of the phase boundary L. Our conclusions are summarized in Table I.

VI. DISCUSSION AND CONCLUSIONS

We leverage the van der Waerden notation, widely used in supersymmetric spinor calculations, to map the low-energy effective Hamiltonian of the Haldane model with Hubbard interaction onto a Lorentz-invariant Lagrangian featuring four-fermion interactions. By solving this model, we unveil two distinct phases: superconducting phase and CDW phase, both driven by the Hubbard interactions. Through this mapping, we establish a connection between high-energy and condensed matter physics, where bilinear quantities and four-Fermi terms in the Lorentz-invariant Lagrangian can be derived in real condensed matter systems, facilitating the emulation of high-energy phenomena in condensed matter systems. For example, the term $\bar{\Psi}_i \mu \gamma^3 \Psi_i$ originates from the chemical potential added to sublattices A and B in the honeycomb lattice, with $\pm\mu$, and $\bar{\Psi}_i m_o \gamma^3 \gamma^5 \Psi_i$ ($m_o = 3\sqrt{3}t' \sin \phi$) arises from next-nearest-neighbor interactions and the magnetic flux. The interaction term: $H_{\text{int}} = \frac{U}{4} [(\Psi^\dagger C \Psi)(\bar{\Psi} C \bar{\Psi}^\dagger) + (\bar{\Psi} \Psi)^2 - (\bar{\Psi} i \gamma^5 \Psi)^2]$ stems from the Hubbard interaction. These mappings substantiate the physical significance of our Lagrangian and its parameters. Our approach provides a methodology to simulate phenomena of interest in high-energy physics within condensed matter systems, thereby fostering a two-way exchange of ideas and techniques between these fields. Such cross fertilization enriches both domains, offering insights into fundamental physical processes. Looking forward, there are several promising avenues for future research. Investigating other two-dimensional lattice models with topological properties [60–70] and exploring their connection to high-energy physics through similar mapping techniques would provide a broader understanding of the interplay between topology and phase transitions in various systems. Extending our approach to

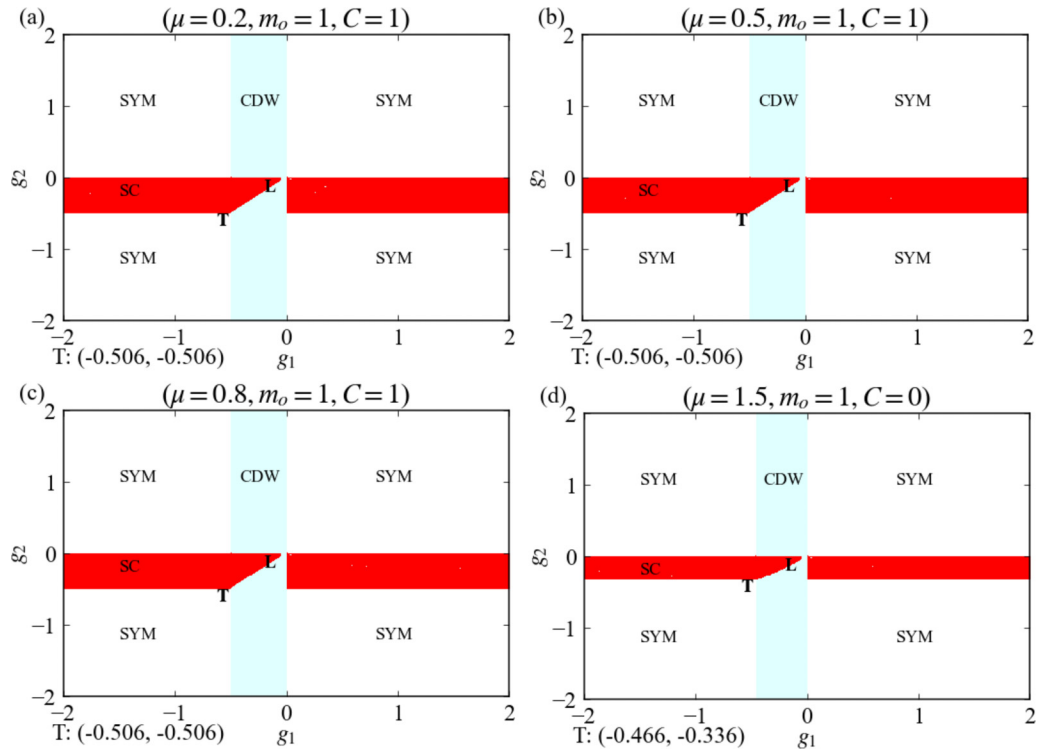


FIG. 5. The (g_1, g_2) -phase portrait for fixed chemical potential and Haldane mass term. Panels (a), (b), and (c) depict the phase diagrams for the topological insulator state ($C = 1$), while panel (d) illustrates the phase diagram for the topologically trivial state. Each diagram is generated by holding the magnitude of m_o constant and progressively increasing the magnitude of μ . The coordinates of the tricritical point T , computed numerically, are provided in the lower-left corner of each figure.

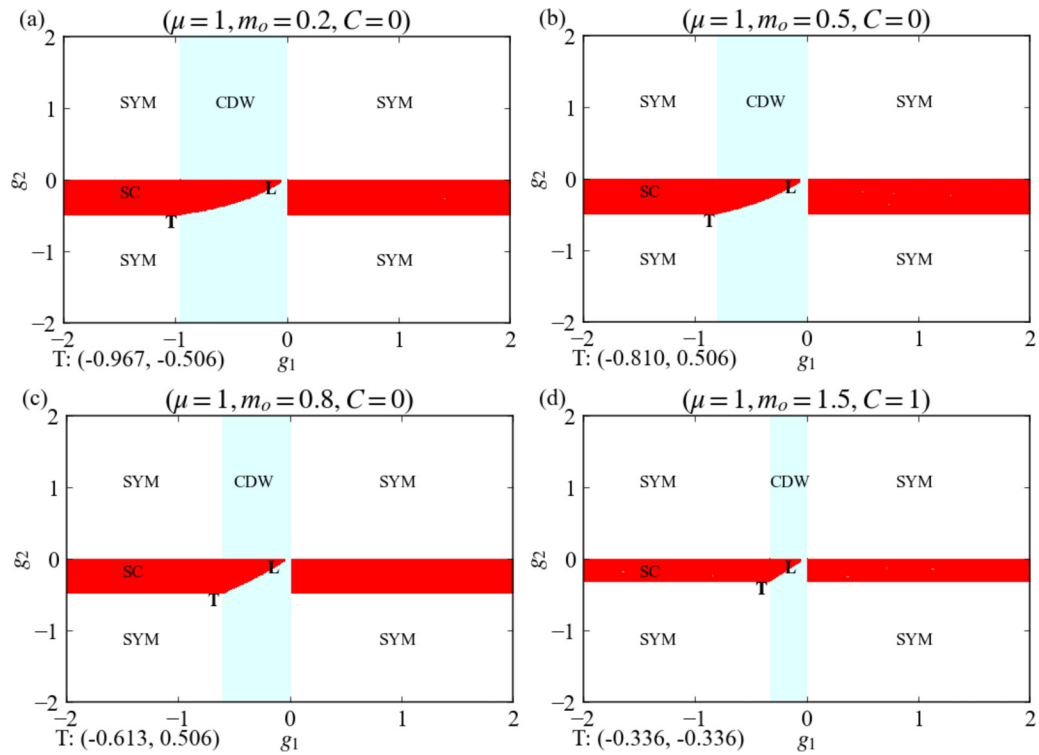


FIG. 6. The (g_1, g_2) -phase portrait for fixed chemical potential and Haldane mass term. Panels (a), (b), and (c) depict the phase diagrams for the topological trivial state ($C = 0$), while panel (d) illustrates the phase diagram for the topologically insulator state. Each diagram is generated by holding the magnitude of μ constant and progressively increasing the magnitude of m_o .

systems with more complex interactions such as long-range couplings could shed light on the emergence of exotic phases and help identify novel materials with unique properties for potential applications in quantum information and nanotechnology.

ACKNOWLEDGMENTS

This work was supported by National Key R&D Program of China under Grants No. 2021YFA1400900, No. 2021YFA0718300, No. 2021YFA1402100, NSFC under Grants No. 12174461, No. 12234012, No. 12247175, No. 12334012, and No. 52327808, Space Application System of China Manned Space Program.

APPENDIX A: ALGEBRA OF THE γ MATRICES

Given that the two spinors in graphene, which are expanded at two inequivalent Dirac points, correspond to left- and right-handed fermions respectively, we adopt the so-called Weyl representation for our gamma algebra here [71,72],

$$\gamma^\mu = \begin{pmatrix} 0 & \bar{\sigma}^\mu \\ \sigma^\mu & 0 \end{pmatrix}, \quad (\text{A1})$$

where $\mu = 0, 1, 2, 3$ and $\bar{\sigma}^\mu = \sigma^\mu$ when $\mu = 0$ and $\bar{\sigma}^\mu = -\sigma^\mu$ when $\mu = 1, 2, 3$ (where σ_0 is the unit 2×2 matrix I). These gamma matrix have the properties $\{\gamma^\mu, \gamma^\nu\} = 2g^{\mu\nu}$, where $g^{\mu\nu} = g_{\mu\nu} = \text{diag}(1, -1, -1, -1)$. There exist another matrix γ^5 , which anticommute with all γ^μ ,

$$\gamma^5 = i\gamma^0\gamma^1\gamma^2\gamma^3 = \begin{pmatrix} -I & 0 \\ 0 & I \end{pmatrix}. \quad (\text{A2})$$

Trace of γ matrices can be evaluated as follows:

$$\begin{aligned} \text{tr}(\mathbf{1}) &= 4, \\ \text{tr}(\text{any odd } \gamma^i\text{'s}) &= 0, \\ \text{tr}(\gamma^\mu\gamma^\nu) &= 4g^{\mu\nu}, \\ \text{tr}(\gamma^\mu\gamma^\nu\gamma^\rho\gamma^\sigma) &= 4(g^{\mu\nu}g^{\rho\sigma} - g^{\mu\rho}g^{\nu\sigma} + g^{\mu\sigma}g^{\nu\rho}), \\ \text{tr}(\gamma^5) &= 0, \\ \text{tr}(\gamma^\mu\gamma^\nu\gamma^5) &= 0, \\ \text{tr}(\gamma^\mu\gamma^\nu\gamma^\rho\gamma^\sigma\gamma^5) &= -4i\epsilon^{\mu\nu\rho\sigma}. \end{aligned} \quad (\text{A3})$$

Contractions of γ matrices with each other simplify to

$$\begin{aligned} \gamma^\mu\gamma_\mu &= 4, \\ \gamma^\mu\gamma^\nu\gamma_\mu &= -2\gamma^\nu, \\ \gamma^\mu\gamma^\nu\gamma^\rho\gamma_\mu &= 4g^{\nu\rho}, \\ \gamma^\mu\gamma^\nu\gamma^\rho\gamma^\sigma\gamma_\mu &= -2\gamma^\sigma\gamma^\rho\gamma^\nu. \end{aligned} \quad (\text{A4})$$

APPENDIX B: PERFORMING THE PATH INTEGRAL OVER THE FERMION

Let us show here some of the details of the path integral over the fermions and which leads to the effective thermodynamic potential. Adopting the procedure described in Refs. [46,47], we assume two anticommuting four component

Dirac spinor fields $q(x)$ and $\bar{q}(x)$. Then, we will calculate the following path integral:

$$I = \int DqD\bar{q} e^{i \int d^3x [\bar{q} D q - \frac{\Delta^*}{2} q^\top C q - \frac{\Delta}{2} \bar{q} C \bar{q}^\top]}, \quad (\text{B1})$$

where $D = i\gamma_\mu\partial_\nu + \mu\gamma^3 + m_o\gamma^3\gamma^5 - \sigma - i\pi\gamma^5$ and $C = -i\gamma^2\gamma^0$ is the charge conjugation matrix. Using the Gaussian path integral identities

$$\int Dp e^{i \int d^3x [-\frac{1}{2} p^\top A p + \eta^\top p]} = (\det A)^{1/2} e^{-\frac{i}{2} \int d^3x \eta^\top A^{-1} \eta}, \quad (\text{B2})$$

and

$$\int D\bar{p} e^{i \int d^3x [-\frac{1}{2} \bar{p} A \bar{p}^\top + \eta \bar{p}^\top]} = (\det A)^{1/2} e^{-\frac{i}{2} \int d^3x \bar{\eta} A^{-1} \bar{\eta}^\top}, \quad (\text{B3})$$

and by also considering $A = \Delta C$, $\bar{q} D = \eta^\top$, $D^\top \bar{q}^\top = \eta$, one finds, after integrating over q and \bar{q} , the result

$$\begin{aligned} I &= \int DqD\bar{q} e^{i \int d^3x [\bar{q} D q - \frac{\Delta^*}{2} q^\top C q - \frac{\Delta}{2} \bar{q} C \bar{q}^\top]} \\ &= [\det(\Delta^2 C^2 + D C^{-1} D^\top C)]^{\frac{1}{2}}, \end{aligned} \quad (\text{B4})$$

where we have assumed $\Delta = \Delta^*$ in the last step. Using the relations $C^{-1}\gamma_\mu^\top C = -\gamma_\mu$ ($\mu = 0, 1, 2, 3$) and $\partial_\mu^\top = -\partial_\mu$, one finds that

$$I = [\det(-\Delta^2 + D_+ D_-)]^{1/2} = (\det B)^{\frac{1}{2}}, \quad (\text{B5})$$

with $D_\pm = i\gamma_\mu\partial_\nu + m_o\gamma^3\gamma^5 - \sigma - i\pi\gamma^5 \pm \mu\gamma^3$. Finally, using the identity $\det B = \exp(\text{Tr} \ln B)$ one finds

$$\ln I = \frac{1}{2} \text{Tr}(\ln B) = \int d^3x \sum_i \int \frac{d^3p}{(2\pi)^3} \ln \lambda_i(p), \quad (\text{B6})$$

where $\lambda_i(p)$ are the eigenvalues of matrix $B(p)$,

$$\begin{aligned} B(p) &= -\Delta^2 + (p_\mu\gamma^\mu + m_o\gamma^3\gamma^5 - \sigma - i\gamma^5\pi + \mu\gamma^3) \\ &\quad \times (p_\mu\gamma^\mu + m_o\gamma^3\gamma^5 - \sigma - i\gamma^5\pi - \mu\gamma^3) \\ &= p^2 - \Delta^2 + m_o^2 + \sigma^2 + \mu^2 \\ &\quad - 2\sigma\boldsymbol{p} - 2\sigma m_o\gamma^3\gamma^5 + 2m_o\boldsymbol{p}\gamma^3\gamma^5 \\ &\quad - 2\mu\boldsymbol{p}\gamma^3 - 2m_o\mu\gamma^5, \end{aligned} \quad (\text{B7})$$

and $\boldsymbol{p} = p^\mu\gamma_\mu$. We first consider the integration over the frequency component p_0 . The eigenvalues λ_i of the matrix $B(p)$ can be expressed as a polynomial in terms of p_0 as follows:

$$\lambda_i(p) = p_0 - \tilde{\lambda}_i(\mathbf{p}), \quad (\text{B8})$$

where

$$\tilde{\lambda}_i(\mathbf{p}) = \begin{cases} \pm \sqrt{\mathbf{p}^2 + (\Delta + m_o + \beta\sqrt{\mu^2 + \sigma^2})^2}, \\ \pm \sqrt{\mathbf{p}^2 + (\Delta - m_o - \beta\sqrt{\mu^2 + \sigma^2})^2}, \end{cases} \quad (\text{B9})$$

and $\beta = \pm$. This implies that p_0 has a total of eight roots.

To integrate the frequency part of Eq. (B6), we employ the formula $\int_{-\infty}^{\infty} dp_0 \ln(p_0 - R) = i\pi |R|$, yielding

$$\begin{aligned} \ln I = & i \int d^3x \sum_{\beta} \int \frac{d^2\mathbf{p}}{(2\pi)^2} \\ & \times (|\sqrt{\mathbf{p}^2 + (\Delta + m_o + \beta\sqrt{\mu^2 + \sigma^2})^2}| \\ & + |\sqrt{\mathbf{p}^2 + (\Delta - m_o - \beta\sqrt{\mu^2 + \sigma^2})^2}|). \end{aligned} \quad (\text{B10})$$

$$\begin{aligned} \Omega^{um}(\Delta, \sigma, \mu, m_o) = & \frac{\sigma^2}{4G} + \frac{\Delta^2}{4G} - \int \frac{d^2\mathbf{p}}{(2\pi)^2} (\sqrt{\mathbf{p}^2 + (\Delta + \sigma)^2} + \sqrt{\mathbf{p}^2 + (\Delta - \sigma)^2}) \\ & - \frac{1}{4} \sum_{\beta, i} \int \frac{d^2\mathbf{p}}{(2\pi)^2} (|p_{0i}^{\beta}| - 4(\sqrt{\mathbf{p}^2 + (\Delta + \sigma)^2} + \sqrt{\mathbf{p}^2 + (\Delta - \sigma)^2})) \\ = & V^{um}(\Delta, \sigma) - \frac{1}{4} \sum_{\beta, i} \int \frac{d^2\mathbf{p}}{(2\pi)^2} (|p_{0i}^{\beta}| - 4(\sqrt{\mathbf{p}^2 + (\Delta + \sigma)^2} + \sqrt{\mathbf{p}^2 + (\Delta - \sigma)^2})). \end{aligned} \quad (\text{B12})$$

The second term on the right-hand side of the above equation is finite, so the renormalization of Ω depends only on the renormalization of the first term. As we have derived in the main text, the renormalized potential is given by $V^{\text{ren}}(\Delta, \sigma) = \frac{\sigma^2}{2\pi g} + \frac{\Delta^2}{2\pi g} + \frac{1}{6\pi}(|\Delta + \sigma|^3 + |\Delta - \sigma|^3)$.

Finally, we can express the renormalized TDP as

$$\begin{aligned} \Omega^{\text{ren}}(\Delta, \sigma) = & \frac{\sigma^2}{2\pi g_1} + \frac{\Delta^2}{2\pi g_2} + \frac{1}{12\pi}(|\Delta + m_o + \sqrt{\mu^2 + \sigma^2}|^3 \\ & + |\Delta + m_o - \sqrt{\mu^2 + \sigma^2}|^3 \\ & + |\Delta - m_o + \sqrt{\mu^2 + \sigma^2}|^3 \\ & + |\Delta - m_o - \sqrt{\mu^2 + \sigma^2}|^3). \end{aligned} \quad (\text{B13})$$

APPENDIX C: USING VAN DER WAERDEN NOTATION TO CONSTRUCT LORENTZ INVARIANTS

In this Appendix we show some of the details for the derivation of bilinear and four fermion terms. In the main text, we let $\Psi = \begin{pmatrix} \eta \\ \chi \end{pmatrix}$, where $\eta = \begin{pmatrix} a_+ \\ b_+ \end{pmatrix}$, $\chi = \begin{pmatrix} a_- \\ b_- \end{pmatrix}$ have the properties of right-chiral and left-chiral Weyl spinor, respectively. So, according to the van der Waerden notation, we use lower-undotted indices to denote the component of the left-chiral Weyl spinor, and use upper-dotted indices with a bar symbol over spinors to denote the components of right-chiral spinors. And we use the Levi-Civita symbol ϵ^{ij} , ϵ_{ij} to raise or lower both dotted and undotted indices [54–56],

$$\begin{aligned} \chi_1 = & b_-, \chi_2 = a_-, \chi^a = \epsilon^{ab} \chi_b, \\ \bar{\eta}^{\dot{1}} = & a_+, \bar{\eta}^{\dot{2}} = b_+, \bar{\eta}^{\dot{a}} = \epsilon^{\dot{a}\dot{b}} \bar{\eta}_{\dot{b}}, \\ \bar{\chi}_{\dot{a}} = & \chi_a^{\dagger}, \bar{\chi}^{\dot{a}} = \chi^{a\dagger}, \bar{\eta}_{\dot{a}} = \eta_a^{\dagger}, \bar{\eta}^{\dot{a}} = \eta^{a\dagger}, \\ \epsilon^{12} = & -\epsilon_{12} = 1. \end{aligned} \quad (\text{C1})$$

Especially, for the right-chiral spinor η , we use $\bar{\eta}$ to denote that we will employ the dot/undot indices, and we use η^{\dagger} to

From this, we can derive the unrenormalized thermodynamic potential (TDP) as

$$\Omega \equiv \Omega^{um}(\Delta, \sigma) = \frac{\sigma^2}{4G} + \frac{\Delta^2}{4G} - \frac{1}{4} \sum_{\beta, i} \int \frac{d^2\mathbf{p}}{(2\pi)^2} |p_{0i}^{\beta}|, \quad (\text{B11})$$

where $p_{0,1}^{\beta} = \sqrt{\mathbf{p}^2 + (\Delta + m_o + \beta\sqrt{\mu^2 + \sigma^2})^2}$ and $p_{0,2}^{\beta} = \sqrt{\mathbf{p}^2 + (\Delta - m_o - \beta\sqrt{\mu^2 + \sigma^2})^2}$.

To renormalize the TDP, we use the following formula:

signify that we will utilize the true components of the Hermitian conjugate of η , i.e., $\eta_1^{\dagger} = a_+^{\dagger}$ and $\bar{\eta}_1 = \epsilon_{12} \bar{\eta}^2 = -b_+$. First, let us deal with the effective chemical potential, the effective chemical potential is

$$H_{\mu} = \mu_A(a_+^{\dagger} a_+ + a_-^{\dagger} a_-) + \mu_B(b_+^{\dagger} b_+ + b_-^{\dagger} b_-). \quad (\text{C2})$$

Using the van der Waerden notation, the first term can be written as

$$\begin{aligned} \mu_A a_+^{\dagger} a_+ = & \frac{\mu_A}{2} (\eta^1 \sigma_{11}^3 \bar{\eta}^{\dot{1}} + \eta^1 \sigma_{11}^0 \bar{\eta}^{\dot{1}} + \eta^2 \sigma_{22}^3 \bar{\eta}^{\dot{2}} + \eta^2 \sigma_{22}^0 \bar{\eta}^{\dot{2}}) \\ = & \frac{\mu_A}{2} (\eta \sigma^3 \bar{\eta} + \eta \sigma^0 \bar{\eta}). \end{aligned} \quad (\text{C3})$$

Similarly, the remaining three can be written as

$$\begin{aligned} \mu_A a_-^{\dagger} a_- = & \frac{\mu_A}{2} (\bar{\chi} \bar{\sigma}^3 \chi + \bar{\chi} \bar{\sigma}^0 \chi), \\ \mu_B b_+^{\dagger} b_+ = & -\frac{\mu_B}{2} (\eta \sigma^3 \bar{\eta} - \eta \sigma^0 \bar{\eta}), \\ \mu_B b_-^{\dagger} b_- = & -\frac{\mu_B}{2} (\bar{\chi} \bar{\sigma}^3 \chi - \bar{\chi} \bar{\sigma}^0 \chi). \end{aligned} \quad (\text{C4})$$

Hence, we obtain

$$\begin{aligned} H_{\mu} = & \frac{\mu_A + \mu_B}{2} (\eta \sigma^0 \bar{\eta} + \bar{\chi} \bar{\sigma}^0 \chi) \\ & + \frac{\mu_A - \mu_B}{2} (\eta \sigma^3 \bar{\eta} + \bar{\chi} \bar{\sigma}^3 \chi). \end{aligned} \quad (\text{C5})$$

We note that the components of the dirac spinors actually is $\Psi = \begin{pmatrix} \eta^{\dot{a}} \\ \chi_a \end{pmatrix}$, and $\bar{\Psi} = (\bar{\chi}_{\dot{a}}, \eta^a)$. So we have $\eta \sigma^{\mu} \bar{\eta} + \bar{\chi} \bar{\sigma}^{\mu} \chi = \bar{\Psi} \gamma^{\mu} \Psi$. Final, the effective chemical potential can be written as

$$H_{\mu} = \frac{\mu_A + \mu_B}{2} \bar{\Psi} \gamma^0 \Psi + \frac{\mu_A - \mu_B}{2} \bar{\Psi} \gamma^3 \Psi. \quad (\text{C6})$$

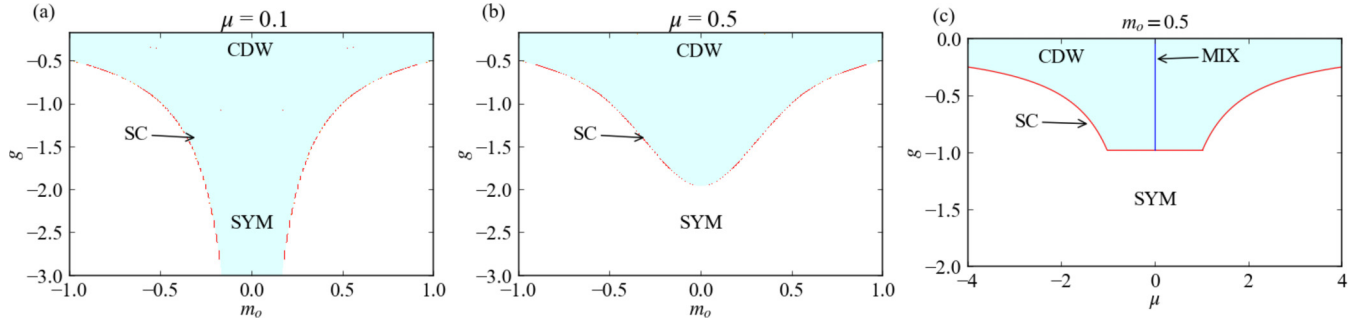


FIG. 7. Phase diagrams in the (g, μ) and (g, m_o) planes for nonzero m_o and μ . (a) and (b) depict the (g, m_o) phase diagrams for $\mu = 0.1$ and $\mu = 0.5$, respectively. (c) illustrates the (g, μ) phase diagram for $m_o = 0.5$.

Second, we deal with the Haldane mass term, $\psi_{\pm}^{\dagger} m_{\pm} \sigma_z \psi_{\pm}$, the sum of these two terms can be written as

$$\begin{aligned} H_o &= \psi_{+}^{\dagger} m_o \sigma_z \psi_{+} + \psi_{-}^{\dagger} (-m_o) \sigma_z \psi_{-} \\ &= m_o (\eta^a \sigma_{ab}^3 \bar{\eta}^b - \bar{\chi}_a \bar{\sigma}^{3ab} \chi_b) \\ &= m_o \bar{\Psi} \gamma^3 \gamma^5 \Psi. \end{aligned} \quad (C7)$$

Finally, we will derive the four-fermion interactions, which are Lorentz invariant. In the main text, we obtain

$$\begin{aligned} H_{\text{int}} &\approx \int d\mathbf{r} U (a_{+}^{\dagger} a_{+} b_{+}^{\dagger} b_{+} + a_{-}^{\dagger} a_{-} b_{-}^{\dagger} b_{-}) \\ &= \int d\mathbf{r} \frac{U}{4} [(\eta \cdot \eta)(\bar{\eta} \cdot \bar{\eta}) + (\bar{\chi} \cdot \bar{\chi})(\chi \cdot \chi)]. \end{aligned} \quad (C8)$$

We note $\Psi^{\dagger} C \Psi = (\eta^{\dagger}, \chi^{\dagger}) \begin{pmatrix} -i\sigma^2 & 0 \\ 0 & i\sigma^2 \end{pmatrix} \begin{pmatrix} \eta \\ \chi \end{pmatrix} = \bar{\eta} \cdot \bar{\eta} + \chi \cdot \chi$ and $\bar{\Psi} \Psi = (\bar{\chi}_a, \eta^a) \begin{pmatrix} \bar{\eta}^a \\ \chi_a \end{pmatrix} = \bar{\chi} \cdot \bar{\eta} + \eta \cdot \chi$. Therefore, we can get

$$\begin{aligned} &(\eta \cdot \eta)(\bar{\eta} \cdot \bar{\eta}) + (\bar{\chi} \cdot \bar{\chi})(\chi \cdot \chi) \\ &= (\bar{\eta} \cdot \bar{\eta} + \chi \cdot \chi)(\bar{\chi} \cdot \bar{\chi} + \eta \cdot \eta) \\ &\quad - \bar{\eta} \cdot \bar{\eta} \bar{\chi} \cdot \bar{\chi} - \chi \cdot \chi \eta \cdot \eta \\ &= (\Psi^{\dagger} C \Psi)(\bar{\Psi} C \bar{\Psi}^{\dagger}) + 2(\eta \cdot \chi)^2 + 2(\bar{\eta} \cdot \bar{\chi})^2 \\ &= (\Psi^{\dagger} C \Psi)(\bar{\Psi} C \bar{\Psi}^{\dagger}) + (\eta \cdot \chi + \bar{\eta} \cdot \bar{\chi})^2 \\ &\quad + (\eta \cdot \chi - \bar{\eta} \cdot \bar{\chi})^2 \\ &= (\Psi^{\dagger} C \Psi)(\bar{\Psi} C \bar{\Psi}^{\dagger}) + (\bar{\Psi} \Psi)^2 - (\bar{\Psi} i \gamma^5 \Psi)^2. \end{aligned} \quad (C9)$$

By the way, if we consider the full effective Hubbard interactions: $\mathcal{H}_F = \int d\mathbf{r} U (a_{+}^{\dagger} a_{+} b_{+}^{\dagger} b_{+} + a_{-}^{\dagger} a_{-} b_{-}^{\dagger} b_{-} + a_{+}^{\dagger} a_{+} b_{-}^{\dagger} b_{-} + a_{-}^{\dagger} a_{-} b_{+}^{\dagger} b_{+})$, we can map this into

$$\mathcal{H} = (\bar{\Psi} \gamma^0 \Psi)^2 - (\bar{\Psi} \gamma^3 \Psi)^2. \quad (C10)$$

Finally, we present the expressions for the charge density wave (CDW) and superconducting (SC) order parameters as derived in the main text,

$$\begin{aligned} \langle \sigma \rangle &= -2 \frac{G}{N} \langle \bar{\Psi} \Psi \rangle = -2 \frac{G}{N} \langle a_{+}^{\dagger} b_{-} + a_{-}^{\dagger} b_{+} + b_{+}^{\dagger} a_{-} + b_{-}^{\dagger} a_{+} \rangle, \\ \langle \Delta \rangle &= -2 \frac{G}{N} \langle \Psi^{\dagger} C \Psi \rangle = -4 \frac{G}{N} \langle a_{+} b_{+} + a_{-} b_{-} \rangle. \end{aligned} \quad (C11)$$

APPENDIX D: (g, μ) , (g, m_o) PHASE DIAGRAMS WHEN $m_o \neq 0$ AND $\mu \neq 0$

This Appendix illustrates the phase diagrams of the system in the (g, μ) and (g, m_o) planes, as illustrated in Fig. 7, given nonzero values of m_o and μ , respectively. The (g, m_o) phase diagram reveals that even for infinitesimally small nonzero chemical potential μ , the system transitions from the initial MIX phase (as described in the main text) to the CDW phase. This observation underscores the pivotal role of μ in driving the system towards the CDW phase, while concurrently suppressing the superconducting phase to a certain extent.

APPENDIX E: REALIZATION PROPOSAL USING ULTRACOLD ATOMS

In a realistic experiment, we note that the realization of the Haldane-Hubbard model is already attainable in cold atoms, and it is possible now to study the quantum phase transitions discussed here. To be specific, we can use a polarized ultracold Fermi gas of ^{40}K atoms, here we choose the hyperfine state $|F, m_F\rangle = |9/2, -7/2\rangle$ by applying certain magnetic fields [73,74], and tunable p -wave interactions have been well implemented utilizing this species of atom in experiments [75–77]. We load the atoms into the honeycomb optical lattice at a wavelength of $\lambda = 826 \text{ nm}$ with potential $V(x, y) = -V_{x1} \sin^2(k_L x) - V_{x2} \cos^2(k_L x) - V_y \cos^2(k_L y) - 2\sqrt{V_{x2} V_y} \cos(k_x) \cos(k_y)$. Here $V_{x1} = 5.0 E_R$, $V_{x2} = 0.46 E_R$ are the lattice depths of two collinear beams along x to create a standing wave, $V_y = 2.2 E_R$ is the lattice depth of the perpendicular beam along y to create a spacing honeycomb lattice, and $k_L = 2\pi/\lambda$. The recoil energy of such an optical lattice is $E_R = \hbar^2/(2m\lambda^2) \approx 7.26 \text{ kHz}$. The frequency detuning between the x_1 and x_2 beams should be set as π , whereas the same frequency for x_2 and y beams, to control the energy offset μ between A-B sublattices. And the phase difference of beams along x and y can control the imaginary part of NNN hopping. Using a Wannier function calculation [78], we extract the amplitude of the NN hopping $t \approx 530 \text{ Hz}$, and the NNN hopping $t' \approx 15 \text{ Hz}$.

Using the technique of p -wave Feshbach resonance, we can obtain Hubbard interaction U as mentioned. The quantum phase transitions here are signaled by the several quasiparticle gaps, which would have dramatic effects on dynamic structure factor that can be measured by Bragg spectroscopy [79–81]. We expect that the charge density wave gap σ and

superconductor gap Δ can be distinguished by different characteristics by spectroscopy measurement.

APPENDIX F: HIGHER-ORDER CORRECTIONS TO THE EFFECTIVE POTENTIAL

To illustrate the efficacy of the mean-field approximation within the large- N framework, we will calculate higher-order corrections to the effective potential. This approach follows the methodology established in [82], which have meticulously explored quantum fluctuations under similar conditions. We aim to prove that quantum fluctuations at zero temperature do not invalidate the saddle-point solutions derived from the mean-field calculations. Specifically, we need to show that the symmetry phase ($\Delta = 0, \sigma = 0$) is not disrupted by quantum fluctuations. For clarity, we will discuss this using the CDW phase as an example.

The Lagrangian we consider is given by

$$\mathcal{L} = \bar{\Psi}_i(i\gamma^v \partial_v + \mu\gamma^3 + m_o\gamma^3\gamma^5 - \sigma)\Psi_i - \frac{N}{4G}\sigma^2. \quad (\text{F1})$$

Upon integrating out the fermionic fields, we obtain the effective action

$$\mathcal{S}_{\text{eff}}[\sigma] = \int d^3x \left(-\frac{N}{4G}\sigma^2 \right) - iN \ln \text{Det}[\mathcal{D}[\sigma]] \quad (\text{F2})$$

where $\text{Det}[\mathcal{D}[\sigma]] = [\sigma^2 + \mu^2 - m_o^2 - p^2]^2 - 4m_o^2p^2$, and $p^2 = p_0^2 - p_1^2 - p_2^2$.

Correspondingly, the effective potential is

$$\Omega_{\text{eff}}(\sigma) = \frac{1}{4G}\sigma^2 + i \int \frac{d^3p}{(2\pi)^3} \times \ln([\sigma^2 + \mu^2 - m_o^2 - p^2]^2 - 4m_o^2p^2). \quad (\text{F3})$$

Our objective is to demonstrate that the symmetry phase is robust against fluctuations. As μ and m_o serve primarily as parameters to control the phase boundaries, for simplicity, we set them to zero and discuss in Euclidean space. The effective potential then becomes

$$\Omega_{\text{eff}}(\sigma) = \frac{1}{4G}\sigma^2 - 2 \int \frac{d^2k}{(2\pi)^2} \int \frac{d\omega}{2\pi} \ln(\omega^2 + k^2 + \sigma^2). \quad (\text{F4})$$

Now let us think about fluctuations. The fluctuations are represented as $\sigma \rightarrow \sigma + \eta$. Integrating out these fluctuations

η , we obtain the modified effective action

$$\tilde{\mathcal{S}}_{\text{eff}}[\sigma] = \mathcal{S}_{\text{eff}}[\sigma] - \text{Tr} \ln \mathcal{A}[\sigma], \quad (\text{F5})$$

where $\mathcal{A}[\sigma]$ is defined as

$$\mathcal{A}[\sigma] = \begin{pmatrix} \frac{\delta^2 S}{\delta\sigma\delta\sigma^*} & \frac{\delta^2 S}{\delta\sigma^2} \\ \frac{\delta^2 S}{\delta\sigma^*2} & \frac{\delta^2 S}{\delta\sigma^*\delta\sigma} \end{pmatrix} [\sigma]. \quad (\text{F6})$$

The corresponding fluctuation-considered effective potential is given by

$$\tilde{\Omega}_{\text{eff}}(\sigma) = \Omega_{\text{eff}}(\sigma) + \Omega_f(\sigma), \quad (\text{F7})$$

where $\Omega_{\text{eff}}(\sigma)$ is provided by Eq. (F3), and $\Omega_f(\sigma)$ is expressed as

$$\Omega_f(\sigma) = - \int \frac{d^2k}{(2\pi)^2} \int \frac{d\omega}{2\pi} \left[\ln \left(\frac{1}{4G} - \alpha(\omega, k) \right) + \ln \left(\frac{1}{4G} - \alpha(\omega, k) + 2\sigma^2\beta(\omega, k) \right) \right], \quad (\text{F8})$$

with $\alpha(\omega, k, \sigma)$ and $\beta(\omega, k, \sigma) = -\frac{\partial\alpha}{\partial\sigma^2}$ defined as

$$\alpha(\omega, k, \sigma) = \int \frac{d^2q}{(2\pi)^2} \int \frac{d\theta}{2\pi} \times \frac{2}{[|q| + i\theta][|q+k| - i(\theta + \omega)] + \sigma^2}. \quad (\text{F9})$$

It is observed that

$$\Omega'_f = |\sigma|V(|\sigma|), \quad (\text{F10})$$

with $V(0)$ being a finite constant, indicating that $\sigma = 0$ is a solution to the gap equation $\tilde{\Omega}'_{\text{eff}}(\sigma) = 0$ with fluctuations considered. The second derivative of the effective potential $\tilde{\Omega}''_{\text{eff}}(\sigma)$ is given by

$$\tilde{\Omega}''_{\text{eff}}(\sigma) = \Omega''_{\text{eff}}(\sigma) + \Omega''_f(\sigma), \quad (\text{F11})$$

Notably, in our calculations for convenience, we set $\hbar = 1$. However, in reality, $\frac{\Omega''_f}{\Omega''_{\text{eff}}} \propto \hbar^2$. Thus, $\Omega''_f(\sigma = 0)$ is significantly smaller than $\Omega''_{\text{eff}}(\sigma = 0)$, implying that $\tilde{\Omega}''_{\text{eff}}(\sigma = 0)$ and $\Omega''_{\text{eff}}(\sigma = 0)$ have the same sign. Therefore, even considering fluctuations, $\sigma = 0$ is indeed a minimum. Similarly, the charge density wave (CDW) solution $\sigma \neq 0$ in the mean-field approach is not nullified by quantum fluctuations, indicating that our zero-temperature phase diagram derived from the mean-field is robust against fluctuations.

[1] A. C. CastroNeto, F. Guinea, N. M. R. Peres, K. S. Novoselov, and A. K. Geim, *Rev. Mod. Phys.* **81**, 109 (2009).
[2] F. D. M. Haldane, *Phys. Rev. Lett.* **61**, 2015 (1988).
[3] T. Neupert, L. Santos, C. Chamon, and C. Mudry, *Phys. Rev. Lett.* **106**, 236804 (2011).
[4] N. Read and D. Green, *Phys. Rev. B* **61**, 10267 (2000).
[5] G. Xu, H. Weng, Z. Wang, X. Dai, and Z. Fang, *Phys. Rev. Lett.* **107**, 186806 (2011).
[6] R. Yu, W. Zhang, H.-J. Zhang, S.-C. Zhang, X. Dai, and Z. Fang, *Science* **329**, 61 (2010).

[7] T. Thonhauser and D. Vanderbilt, *Phys. Rev. B* **74**, 235111 (2006).
[8] C.-Z. Chang, J. Zhang, X. Feng, J. Shen, Z. Zhang, M. Guo, K. Li, Y. Ou, P. Wei, L.-L. Wang *et al.*, *Science* **340**, 167 (2013).
[9] I. F. Herbut, *Phys. Rev. Lett.* **97**, 146401 (2006).
[10] I. F. Herbut, V. Juričić, and B. Roy, *Phys. Rev. B* **79**, 085116 (2009).
[11] C. Hickey, L. Cincio, Z. Papić, and A. Paramekanti, *Phys. Rev. Lett.* **116**, 137202 (2016).

- [12] T. I. Vanhala, T. Siro, L. Liang, M. Troyer, A. Harju, and P. Törmä, *Phys. Rev. Lett.* **116**, 225305 (2016).
- [13] L. M. Cangemi, A. S. Mishchenko, N. Nagaosa, V. Cataudella, and G. De Filippis, *Phys. Rev. Lett.* **123**, 046401 (2019).
- [14] T.-C. Yi, S. Hu, E. V. Castro, and R. Mondaini, *Phys. Rev. B* **104**, 195117 (2021).
- [15] J.-J. Miao, D.-H. Xu, L. Zhang, and F.-C. Zhang, *Phys. Rev. B* **99**, 245154 (2019).
- [16] P. Mai, B. E. Feldman, and P. W. Phillips, *Phys. Rev. Res.* **5**, 013162 (2023).
- [17] T. H. Yanes, M. Płodzień, M. M. Sinkevičienė, G. Žlabys, G. Juzeliūnas, and E. Witkowska, *Phys. Rev. Lett.* **129**, 090403 (2022).
- [18] P. Castro, D. Shaffer, Y.-M. Wu, and L. H. Santos, *Phys. Rev. Lett.* **131**, 026601 (2023).
- [19] I. F. Herbut and S. Mandal, *Phys. Rev. B* **108**, L161108 (2023).
- [20] I. F. Herbut, [arXiv:2304.07654](https://arxiv.org/abs/2304.07654).
- [21] G. Palumbo and J. K. Pachos, *Phys. Rev. D* **90**, 027703 (2014).
- [22] G. Palumbo and J. K. Pachos, *Phys. Rev. Lett.* **110**, 211603 (2013).
- [23] M. Cirio, G. Palumbo, and J. K. Pachos, *Phys. Rev. B* **90**, 085114 (2014).
- [24] L. Fernández, V. S. Alves, M. Gomes, L. O. Nascimento, and F. Peña, *Phys. Rev. D* **103**, 105016 (2021).
- [25] L. Fernández, V. S. Alves, L. O. Nascimento, F. Peña, M. Gomes, and E. C. Marino, *Phys. Rev. D* **102**, 016020 (2020).
- [26] V. S. Alves, R. O. C. Junior, E. C. Marino, and L. O. Nascimento, *Phys. Rev. D* **96**, 034005 (2017).
- [27] T. G. Khunjua, K. G. Klimenko, R. N. Zhokhov, and V. C. Zhukovsky, *Phys. Rev. D* **95**, 105010 (2017).
- [28] T. G. Khunjua, K. G. Klimenko, and R. N. Zhokhov, *Phys. Rev. D* **98**, 054030 (2018).
- [29] T. G. Khunjua, K. G. Klimenko, and R. N. Zhokhov, *Phys. Rev. D* **100**, 034009 (2019).
- [30] D. Ebert, H. Reinhardt, and M. Volkov, *Prog. Part. Nucl. Phys.* **33**, 1 (1994).
- [31] M. Buballa, *Phys. Rep.* **407**, 205 (2005).
- [32] J. Li, G. Cao, and L. He, *Phys. Rev. D* **104**, 074026 (2021).
- [33] D. Ebert, K. G. Klimenko, and H. Toki, *Phys. Rev. D* **64**, 014038 (2001).
- [34] D. Ebert, V. V. Khudiyakov, V. C. Zhukovsky, and K. Klimenko, *Phys. Rev. D* **65**, 054024 (2002).
- [35] D. Ebert and K. G. Klimenko, *Phys. Rev. D* **82**, 025018 (2010).
- [36] D. Ebert, N. V. Gubina, K. G. Klimenko, S. Kurbanov, and V. C. Zhukovsky, *Phys. Rev. D* **84**, 025004 (2011).
- [37] D. Ebert, T. G. Khunjua, K. G. Klimenko, and V. C. Zhukovsky, *Phys. Rev. D* **90**, 045021 (2014).
- [38] D. Ebert, T. G. Khunjua, K. G. Klimenko, and V. C. Zhukovsky, *Phys. Rev. D* **91**, 105024 (2015).
- [39] T. G. Khunjua, K. G. Klimenko, and R. Zhokhov, *Phys. Rev. D* **106**, 085002 (2022).
- [40] M. M. Gubaeva, T. G. Khunjua, K. G. Klimenko, and R. N. Zhokhov, *Phys. Rev. D* **106**, 125010 (2022).
- [41] H. Gies and L. Janssen, *Phys. Rev. D* **82**, 085018 (2010).
- [42] M. Gomes, R. S. Mendes, R. F. Ribeiro, and A. J. da Silva, *Phys. Rev. D* **43**, 3516 (1991).
- [43] A. Giuliani, I. Jauslin, V. Mastropietro, and M. Porta, *Phys. Rev. B* **94**, 205139 (2016).
- [44] D. Dudal, A. J. Mizher, and P. Pais, *Phys. Rev. D* **98**, 065008 (2018).
- [45] J. A. C. Olivares, L. Albino, A. J. Mizher, and A. Raya, *Phys. Rev. D* **102**, 096023 (2020).
- [46] D. Ebert, T. G. Khunjua, K. G. Klimenko, and V. C. Zhukovsky, *Phys. Rev. D* **93**, 105022 (2016).
- [47] K. G. Klimenko, R. N. Zhokhov, and V. C. Zhukovsky, *Phys. Rev. D* **86**, 105010 (2012).
- [48] Y. M. P. Gomes and R. O. Ramos, *Phys. Rev. B* **104**, 245111 (2021).
- [49] Y. M. P. Gomes and R. O. Ramos, *Phys. Rev. B* **107**, 125120 (2023).
- [50] M. E. Carrington, *Phys. Rev. B* **99**, 115432 (2019).
- [51] V. Gusynin, S. Sharapov, and J. Carbotte, *Int. J. Mod. Phys. B* **21**, 4611 (2007).
- [52] X. Luo, Y. Yu, and L. Liang, *Phys. Rev. B* **91**, 125126 (2015).
- [53] X. Luo, Y. Lan, Y. Yu, and L. Liang, *Phys. Rev. Lett.* **114**, 249101 (2015).
- [54] H. J. Muller-Kirsten and A. Wiedemann, *Introduction to Supersymmetry* (World Scientific, Singapore, 2010), Vol. 80.
- [55] P. Labelle, *Supersymmetry Demystified* (McGraw Hill, London, 2010).
- [56] S. P. Martin, in *Perspectives on Supersymmetry II* (World Scientific, Singapore, 2010), pp. 1–153.
- [57] E. Zhao and A. Paramekanti, *Phys. Rev. Lett.* **97**, 230404 (2006).
- [58] M. Iskin, *Phys. Rev. A* **99**, 023608 (2019).
- [59] A. Cichy and A. Ptok, *Phys. Rev. A* **97**, 053619 (2018).
- [60] F. Sun, X.-L. Yu, J. Ye, H. Fan, and W.-M. Liu, *Sci. Rep.* **3**, 2119 (2013).
- [61] F. Sun and J. Ye, [arXiv:2303.06541](https://arxiv.org/abs/2303.06541).
- [62] F. Sun and J. Ye, [arXiv:2303.07251](https://arxiv.org/abs/2303.07251).
- [63] P. C. Klipstein, *Phys. Rev. B* **104**, 195407 (2021).
- [64] C.-Z. Chen, H. Liu, H. Jiang, Q.-F. Sun, Z. Wang, and X. C. Xie, *Phys. Rev. B* **91**, 214202 (2015).
- [65] P.-L. Zhao, X.-B. Qiang, H.-Z. Lu, and X. C. Xie, *Phys. Rev. Lett.* **127**, 176601 (2021).
- [66] C.-A. Li, B. Fu, Z.-A. Hu, J. Li, and S.-Q. Shen, *Phys. Rev. Lett.* **125**, 166801 (2020).
- [67] X. Li, Q. Niu and Q. Niu, *Phys. Rev. B* **95**, 241411(R) (2017).
- [68] C. H. Lee and X.-L. Qi, *Phys. Rev. B* **90**, 085103 (2014).
- [69] G.-F. Zhang, Y. Li, and C. Wu, *Phys. Rev. B* **90**, 075114 (2014).
- [70] F. Yang, S.-J. Jiang, and F. Zhou, *Phys. Rev. B* **100**, 054508 (2019).
- [71] M. Peskin, *An Introduction to Quantum Field Theory* (CRC Press, Boca Raton, FL, 2018).
- [72] M. Srednicki, *Quantum Field Theory* (Cambridge University Press, Cambridge, 2007).
- [73] L. Tarruell, D. Greif, T. Uehlinger, G. Jotzu, and T. Esslinger, *Nature (London)* **483**, 302 (2012).
- [74] G. Jotzu, M. Messer, R. Desbuquois, M. Lebrat, T. Uehlinger, D. Greif, and T. Esslinger, *Nature (London)* **515**, 237 (2014).
- [75] C. A. Regal, C. Ticknor, J. L. Bohn, and D. S. Jin, *Phys. Rev. Lett.* **90**, 053201 (2003).
- [76] K. Günter, T. Stöferle, H. Moritz, M. Köhl, and T. Esslinger, *Phys. Rev. Lett.* **95**, 230401 (2005).
- [77] C. Ticknor, C. A. Regal, D. S. Jin, and J. L. Bohn, *Phys. Rev. A* **69**, 042712 (2004).
- [78] T. Uehlinger, G. Jotzu, M. Messer, D. Greif, W. Hofstetter, U. Bissbort, and T. Esslinger, *Phys. Rev. Lett.* **111**, 185307 (2013).

- [79] J. M. Vogels, K. Xu, C. Raman, J. R. Abo-Shaeer, and W. Ketterle, *Phys. Rev. Lett.* **88**, 060402 (2002).
- [80] D. Clément, N. Fabbri, L. Fallani, C. Fort, and M. Inguscio, *Phys. Rev. Lett.* **102**, 155301 (2009).
- [81] P. T. Ernst, S. Götze, J. S. Krauser, K. Pyka, D.-S. Lühmann, D. Pfannkuche, and K. Sengstock, *Nat. Phys.* **6**, 56 (2010).
- [82] E. Marino and L. H. Nunes, *Nucl. Phys. B* **741**, 404 (2006).